Planar magnetic texture on the surface of a topological insulator

Zhaochen Liu,[1] Jing Wang,[1,2,3,*] and Congjun Wu[4,5,6,7,†]

[1]*State Key Laboratory of Surface Physics and Department of Physics, Fudan University, Shanghai 200433, China*
[2]*Institute for Nanoelectronic Devices and Quantum Computing, Fudan University, Shanghai 200433, China*
[3]*Zhangjiang Fudan International Innovation Center, Fudan University, Shanghai 201210, China*
[4]*Department of Physics, School of Sciences, Westlake University, Hangzhou 310024, Zhejiang, China*
[5]*Institute for Theoretical Sciences, Westlake University, Hangzhou 310024, Zhejiang, China*
[6]*Key Laboratory for Quantum Materials of Zhejiang Province, School of Science, Westlake University, Hangzhou 310024, China*
[7]*Institute of Natural Sciences, Westlake Institute for Advanced Study, Hangzhou 310024, Zhejiang, China*

(Received 8 November 2021; revised 9 March 2022; accepted 5 July 2022; published 20 July 2022)

We study the planar magnetic textures coupled to a two-dimensional Dirac surface state, where both the magnetic texture and surface state form in the magnetic topological insulator surface layer. It is shown that the radial vortex with winding number $w = \pm 1$ leads to the confinement of Dirac states, where a mapping to the Schrödinger equation of a two-dimensional hydrogen atom is found. The fully spin-polarized zero-energy bound state forms a flat band that resembles the zeroth Landau level of Dirac electrons in a uniform out-of-plane magnetic field. Remarkably, the number of the zero-energy state is topologically robust. Interestingly, when such a system is proximity coupled to an s-wave superconductor, the existence of Majorana zero modes at the Abrikosov vortex depends only on the relative value of the magnetic exchange coupling and the pairing strength. We conclude with a brief discussion on the physical realization with such magnetic textures.

DOI: 10.1103/PhysRevB.106.035134

I. INTRODUCTION

Topology has become a central theme in condensed matter physics. Interesting quantum phenomena emerge from the intricate interplay between nontrivial topology and magnetism [1–5]. Two outstanding examples are the quantum anomalous Hall effect and axion insulators discovered in magnetic topological insulators (TIs) [6–20]. The exchange coupling between an out-of-plane magnetization and the TI surface state opens a gap in the surface spectrum. The gap opening is accompanied by the emergence of the surface quantum Hall effect with a half-quantized Hall conductance described by the axion electrodynamics [6], which is the physical origin of the topological magnetoelectric effect. It leads to rich phenomena such as the quantum anomalous Hall effect with a chiral edge state emerging at the magnetic domain wall as well as the topological magneto-optical effect [21–23].

Peculiar physics emerges when the Dirac surface states couple to spatially nonuniform magnetic textures, such as skyrmions and domain walls [5,24–29]. In this paper, we study theoretically the two-dimensional (2D) magnetic textures, formed in the surface layer of an intrinsic magnetic TI coupled to TI surface states. A Dirac electron with a radial magnetic vortex with a winding number $w = \pm 1$ can be exactly mapped to the Schrödinger equation of a 2D hydrogen atom. The fully spin-polarized zero-energy bound state resembles the zeroth Landau level of Dirac electrons in a uniform out-of-plane magnetic field. The radial magnetic vortex acts effectively as a magnetic field along the z axis with $1/r$ dependence. Interestingly, when the system is coupled to an s-wave superconductor, the existence of emergent Majorana bound states at the Abrikosov vortex core depends only on the relative value of the magnetic exchange coupling and the pairing strength.

The remainder of this paper is organized as follows. Section II introduces the effective model for surface Dirac electrons coupled to the planar magnetic texture. Section III presents the analytic and numerical calculations of the energy spectrum for radial and curling vortices, respectively. Section IV presents results when the system is proximity coupled to an s-wave superconductor. Section V discusses the physical realization of a planar magnetic texture. Some auxiliary materials are relegated to the Supplemental Material (SM).

II. MODEL

The planar magnetic texture we consider exhibits the form of $\mathbf{S}(\mathbf{r}) \equiv S\mathbf{n}(\mathbf{r}) = S[\cos\vartheta(\mathbf{r}), \sin\vartheta(\mathbf{r}), 0]$, where $\mathbf{n}(\mathbf{r})$ is the unit vector describing the magnetization direction, and $\mathbf{r} = (x, y)$. It is characterized by the topological winding number [30]

$$w = \frac{1}{2\pi}\oint \nabla\vartheta \cdot d\mathbf{r}. \tag{1}$$

Two typical magnetic vortices with $w = 1$ are illustrated in Figs. 1(a) and 1(b).

In the presence of the magnetic vortex $\mathbf{n}(\mathbf{r})$ on the magnetic TI surface layer, the surface states of a magnetic TI can be

*wjingphys@fudan.edu.cn
†wucongjun@westlake.edu.cn

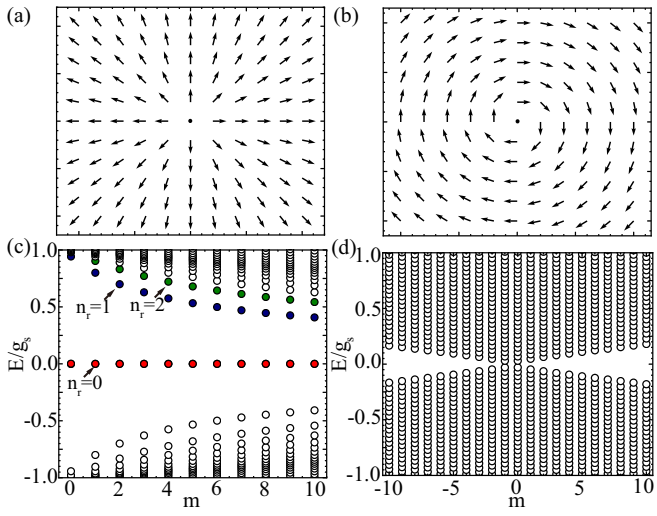

FIG. 1. (a), (b) Schematics of the radial and curling planar magnetic vortices in Eqs. (5) and (11), respectively. The vector field represents the direction of local magnetization $\mathbf{n}(\mathbf{r})$. (c), (d) The numerically calculated energy spectrum for the two cases in (a) and (b) with $g_s = 2$, $v_F = 10$, respectively. The bound-state spectrum in (c) is bounded by $|E_\pm| < g_s$.

described by the Dirac Hamiltonian

$$\mathcal{H} = v_F(\mathbf{k} \times \boldsymbol{\sigma}) \cdot \hat{\mathbf{e}}_z + g_s \mathbf{n}(\mathbf{r}) \cdot \boldsymbol{\sigma}. \tag{2}$$

Here, $\hbar \equiv 1$, v_F is the Fermi velocity, $\hat{\mathbf{e}}_z$ is the unit vector normal to the surface, and $\boldsymbol{\sigma} = (\sigma_x, \sigma_y, \sigma_z)$ are the Pauli matrices describing the spin. $g_s \equiv J'S\rho_s/2$, J' is the exchange interaction between the local spin and surface electron, and ρ_s is the sheet density of local spin. Without loss of generality, we set $g_s/v_F > 0$ and neglect the particle-hole asymmetry.

We notice that the in-plane Zeeman term is equivalent to a vector potential, thus the Hamiltonian becomes

$$\mathcal{H} = v_F[(\mathbf{k} - \boldsymbol{\mathcal{A}}) \times \boldsymbol{\sigma}] \cdot \hat{\mathbf{e}}_z, \tag{3}$$

where $\boldsymbol{\mathcal{A}}(\mathbf{r}) \equiv (g_s/v_F)[-\sin\vartheta(\mathbf{r}), \cos\vartheta(\mathbf{r})]$. For a generic $\boldsymbol{\mathcal{A}}(\mathbf{r})$, Eq. (3) is difficult to solve analytically. In the following, we assume $\mathbf{n}(\mathbf{r})$ is rotationally invariant along the z axis. The Hamiltonian conserves the total angular momentum, and the energy spectrum can be obtained analytically by squaring $\mathcal{H}$ to solve $\mathcal{H}^2\psi = E^2\psi$, which is

$$\mathcal{H}^2/v_f^2 = -\nabla^2 + \boldsymbol{\mathcal{A}}^2 + 2i\boldsymbol{\mathcal{A}} \cdot \nabla + i(\nabla \cdot \boldsymbol{\mathcal{A}}) - \nabla \times \boldsymbol{\mathcal{A}} \cdot \boldsymbol{\sigma}. \tag{4}$$

In terms of the 2D polar coordinates (r, ϕ), Eq. (4) may be separated into radial and angular parts. Two typical magnetic textures are radial and curling vortices.

III. ENERGY SPECTRUM

A. Radial vortex

First, we consider a radial magnetic vortex illustrated in Fig. 1(a),

$$\mathbf{n}_1(\mathbf{r}) = \hat{\mathbf{e}}_r = \frac{1}{r}(x\hat{\mathbf{e}}_x + y\hat{\mathbf{e}}_y), \tag{5}$$

where $r = \sqrt{x^2 + y^2}$. Now $\boldsymbol{\mathcal{A}}_1(\mathbf{r}) \equiv (g_s/v_F)(-y/r, x/r)$, and $\nabla \cdot \boldsymbol{\mathcal{A}}_1 = 0$, $\nabla \times \boldsymbol{\mathcal{A}}_1 = (g_s/v_F)(\hat{\mathbf{e}}_z/r)$, $\nabla \cdot \nabla \times \boldsymbol{\mathcal{A}}_1 = 0$, and $\boldsymbol{\mathcal{A}}_1 \cdot \nabla = -(g_s/v_F)(y\partial_x - x\partial_y)/r \equiv (g_s/v_F)(iL_z/r)$, with L_z the orbital angular momentum operator. Then Eq. (4) becomes

$$\frac{\mathcal{H}_1^2}{v_F^2} = -\frac{1}{r}\partial_r(r\partial_r) + \frac{L_z^2}{r^2} - \frac{g_s}{v_F r}(2L_z + \sigma_z) + \frac{g_s^2}{v_F^2}, \tag{6}$$

where $\partial_r \equiv \partial/\partial r$.

Since $[L_z, \mathcal{H}_1^2] = 0$, the eigenfunction of $\mathcal{H}_1^2$ must have the form as $\varphi(r, \phi) = e^{im\phi} f(r)$, where the orbital momentum quantum number $m = 0, \pm 1, \pm 2, \ldots$ is connected with the total angular momentum $j = m + 1/2$. The radial wave function satisfies the equation

$$\left[\frac{1}{r}\partial_r(r\partial_r) - \frac{m^2}{r^2} + \frac{g_s}{v_F r}(2m \pm 1) - \frac{g_s^2}{v_F^2} + \frac{E^2}{v_F^2}\right] f(r) = 0. \tag{7}$$

Here, $\pm$ denote $|\uparrow\rangle$ and $|\downarrow\rangle$ with $\sigma_z = +1$ and $\sigma_z = -1$, respectively. We define the dimensionless quantities

$$r' = r\frac{g_s}{v_F}(m \pm 1/2), \quad E' = \frac{(E/g_s)^2 - 1}{2(m \pm 1/2)^2}. \tag{8}$$

Then Eq. (7) has the exact form as the Schrödinger equation of a 2D hydrogen atom [31], which is the main result of this paper,

$$\left[\frac{\partial^2}{\partial r'^2} + \frac{1}{r'}\frac{\partial}{\partial r'} - \frac{m^2}{r'^2} + \left(2E' + \frac{2}{r'}\right)\right] f(r') = 0. \tag{9}$$

Equation (9) can be solved algebraically due to the hidden dynamical symmetry of the hydrogen atom [32], which is related to the conserved Runge-Lenz operator $\mathbf{K} \equiv -(i\nabla \times \mathbf{L}_z - \mathbf{L}_z \times i\nabla) - 2\hat{\mathbf{e}}_r$, satisfying $[\mathcal{H}^2, \mathbf{K}] = \mathbf{0}$, $[L_z, K_x] = iK_y$, $[L_z, K_y] = -iK_x$, and $[K_x, K_y] = -4iL_z\mathcal{H}_1^2$.

Now $r' > 0$ corresponds to an attractive Coulomb potential, which contains both bound discrete states and unbound continuous states. For $m \geqslant 0$, the eigenvalue of the bound states in Eq. (7) is $E' = -1/2n_2^2$, where the principle quantum number $n_2 \equiv n_r + |m| + 1/2$, with $n_r = 0, 1, 2, \ldots$. The radial wave function $f_{n_r,m}(r') = r'^{|m|}e^{-r'/n_2}F(-n_r, 2|m| + 1, 2r'/n_2)$, with $F(\alpha, \gamma; x)$ the confluent hypergeometric function. The spinor wave function of $\mathcal{H}_1$ is obtained by noticing that the degeneracy between $|\uparrow\rangle$ and $|\downarrow\rangle$ exists when $n_{r,\uparrow} = n_{r,\downarrow} + 1$ and $m_{r,\uparrow} = m_{r,\downarrow} - 1$, namely $E_{+,n_r,m} = E_{-,n_r-1,m+1}$. Explicitly, the energy spectrum and (un-normalized) spinor wave function of bound states of $\mathcal{H}_1$ are

$$\frac{E_\pm}{g_s} = \pm\left(1 - \frac{(m + \frac{1}{2})^2}{n_2^2}\right)^{\frac{1}{2}},$$
$$\psi_\pm = \begin{pmatrix} e^{im\phi} f_{n_r,m}(r'_+) \\ \mp\frac{\sqrt{(n_r+m+1)n_r}}{(m+1)(2m+1)n_2} e^{i(m+1)\phi} f_{n_r-1,m+1}(r'_-) \end{pmatrix}. \tag{10}$$

The bound-state energies are within the interval between $\pm g_s$. The maximum of radial probability density is located at $r_{\max} \approx n_2^2 a/(m \pm 1/2)$, with Bohr radius $a \equiv \hbar v_F/g_s$. For $m < 0$ (and $r' < 0$), Eq. (9) corresponds to a repulsive Coulomb potential, so there are no bound states, and the continuous energy spectrum satisfies $E' \geqslant 0$, namely $|E| \geqslant g_s$.

The branch of states with $n_r = 0$ are zero-energy states and fully spin polarized as shown in their wave functions $\psi = [e^{im\phi} f_{0,m}(r'_+), 0]^T$. They form a flat band resembling the spin-polarized zeroth Landau level of Dirac fermions in

a uniform magnetic field. However, the magnetic translation symmetry is absent here since $\nabla \times \boldsymbol{\mathcal{A}}_1$ scales as $1/r$. Consequently, the density of states of the zero-energy states scales as $1/r$ away from the center, consistent with the classic radius $r_m = (m + 1/2)a$. This situation is similar to the Landau level formation of a 2D Rashba system subject to a harmonic potential [33,34]. It is worth mentioning that the confinement of the Dirac surface state subjected to 3D magnetic skyrmions has been studied previously [28,29]. However, the main difference here for a Dirac surface state coupled to a 2D radial magnetic vortex is the emergence of a zero-energy bound state, where the number of such zero-energy states is *topologically robust*, which equals $\mathcal{N} - 1$ with $\mathcal{N}$ the closest integer to the total flux in units of flux quantum, as an application of the Atiyah-Singer index theorem to the 2D Dirac equation [35].

The analytic solutions of the energy spectrum are further confirmed by the numerical calculation in Fig. 1(c). Here, we choose a disk geometry, and the radial wave function is expanded in terms of the Bessel function [36], the expanding order, and the disk radius $\mathcal{R}$ is large enough to ensure convergence and capture the low-energy states [37].

B. Curling vortex

Next, we consider a curling magnetic vortex shown in Fig. 1(b),

$$\mathbf{n}_2(\mathbf{r}) = \hat{\mathbf{e}}_\phi = \frac{1}{r}(y\hat{\mathbf{e}}_x - x\hat{\mathbf{e}}_y). \tag{11}$$

Then $\boldsymbol{\mathcal{A}}_2(\mathbf{r}) = (g_s/v_F)(x/r, y/r)$, with a zero emergent magnetic field $\nabla \times \boldsymbol{\mathcal{A}}_2 = \mathbf{0}$ and $\nabla \cdot \boldsymbol{\mathcal{A}}_2 = (g_s/v_F)(1/r)$. Interestingly, the curling texture can be gauged away, i.e., $\boldsymbol{\mathcal{A}}_2 \to \boldsymbol{\mathcal{A}}_2' + (g/v_F)\nabla r$ and $\psi \to \psi' \exp(igr/v_F)$. There are no bound-state solutions but only continuous-state solutions [37]. The energy spectrum is numerically calculated in Fig. 1(d).

IV. MAJORANA BOUND STATE

It is well known that the localized Majorana zero modes (MZMs) arise in the Abrikosov vortex core when TI Dirac surface states are proximity coupled to an *s*-wave superconductor [38–43]. Skyrmion-induced bound states in superconductors have been studied previously [44,45]. Now we study the fate of MZMs in the presence of a 2D magnetic texture on a TI surface.

Here, we consider a bilayer heterostructure with an *s*-wave superconductor and magnetic TI, where a magnetic texture is assumed to form on the intrinsic magnetic TI surface layer. Now the pairing term $V = \Delta(\mathbf{r})\psi_\uparrow^\dagger \psi_\downarrow^\dagger + \text{H.c.}$ is added to $\mathcal{H}$, where $\Delta(\mathbf{r})$ is the superconducting proximity-induced pairing potential on a surface state. The system can be diagonalized with the Bogoliubov transformation

$$\psi_\sigma(\mathbf{r}) = \sum_n [u_{n,\sigma}(\mathbf{r})\gamma_n + v_{n,\sigma}^*(\mathbf{r})\gamma_n^\dagger], \tag{12}$$

where $\gamma_n^\dagger$ creates a Bogoliubov quasiparticle. Then the resulting Bogoliubov–de Gennes (BdG) equation is

$$\begin{pmatrix} \mathcal{H} - \mu & \Delta(\mathbf{r}) \\ \Delta^*(\mathbf{r}) & -\sigma_y \mathcal{H}^* \sigma_y + \mu \end{pmatrix} \Phi_n(\mathbf{r}) = E_n \Phi_n(\mathbf{r}), \tag{13}$$

with the BdG energy spectrum E_n and Nambu wave function $\Phi_n(\mathbf{r}) = [u_{n\uparrow}(\mathbf{r}), u_{n\downarrow}(\mathbf{r}), v_{n\downarrow}(\mathbf{r}), -v_{n\uparrow}(\mathbf{r})]^T$.

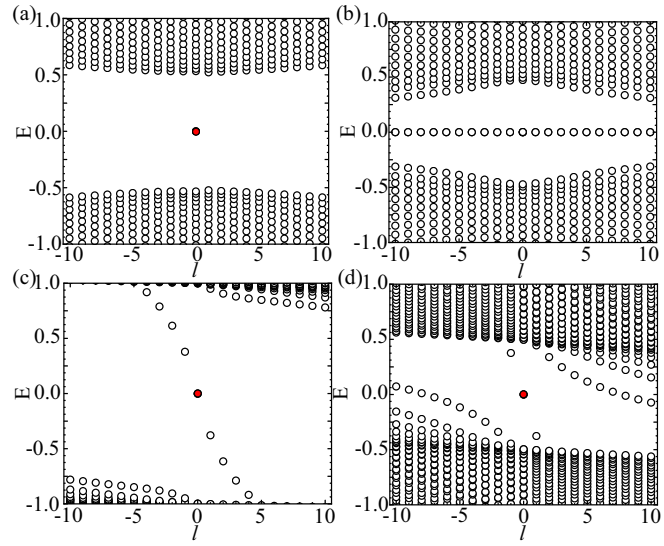

FIG. 2. The BdG energy spectrum of the Abrikosov vortex $\Delta_0(r)e^{i\theta}$ for radial vortex texture. (a) $g_s = 0.5$, $\mu = 0$, $\Delta_0 = 1.0$. (b) $g_s = 1.0$, $\mu = 0$, $\Delta_0 = 0.5$. (c) $g_s = 0.5$, $\mu = 5.0$, $\Delta_0 = 1.0$. (d) $g_s = 1.0$, $\mu = 5.0$, $\Delta_0 = 0.5$. We set $v_F = 10$.

The BdG equation can be solved numerically for a general pairing potential. Here, for simplicity we assume $\Delta(\mathbf{r})$ for a surface state that has the form of an Abrikosov vortex, where the origin of the vortex core coincides with the center of the magnetic texture as in Fig. 3(a), and the effective magnetic flux is contributed by the radial magnetic vortex on the surface layer. We mention that the spin moment from the magnetic texture acts as an effective gauge field, the curl of which must fulfill the requirement to exceed a lower critical field in order to generate a vortex in the superconductor. Otherwise, this may further limit the exact form of the pairing potential presented here. Now Eq. (13) has a cylindrical symmetry. In the polar coordinate, the pairing potential with a vortex is $\Delta(\mathbf{r}) = \Delta_0(r)e^{i\theta} = \Delta_0 \tanh(r/\epsilon_0)e^{i\theta}$, where ϵ_0 characterizes the size of the vortex core. The wave function can be factorized into

$$\Phi_{n,\ell} = e^{i\ell\theta}(u_{n,\ell\uparrow}, u_{n,\ell+1\downarrow}e^{i\theta}, v_{n,\ell-1\downarrow}e^{-i\theta}, -v_{n,\ell\uparrow})^T,$$

where the principle quantum number n is determined by solving the radial equation in the basis of a Bessel function. The details of the numerical calculations are given in the Supplemental Material [37]. The calculation is performed on a disk of radius $\mathcal{R} = 40\epsilon_0$.

Figure 2 shows the numerical results of the BdG energy spectrum for a radial vortex. The MZM is denoted as a red dot. As shown in Figs. 2(a) and 2(b) for $\mu = 0$, the existence of a MZM depends only on the relative value of the magnetic coupling g_s and pairing strength Δ_0, namely a MZM exists for $g_s < \Delta_0$ and disappears for $g_s > \Delta_0$. The zero-energy states in Fig. 2(b) are not MZMs, but originate from the zero-energy bound states in Fig. 1(c), which deviate from zero by adding a small Zeeman term $\Delta_z\sigma_z$ into $\mathcal{H}$. These results can be simply understood that for $\mu = 0$, the chemical potential resides in the bound-state spectrum. Only when the pairing potential exceeds the bound-state energy and reaches the continuous state,

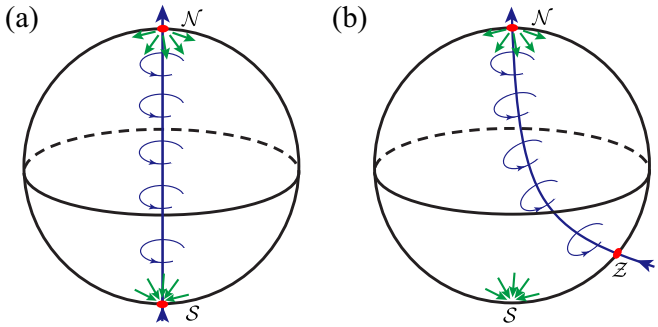

FIG. 3. (a), (b) The MZMs are trapped near the surface in the Abrikosov vortex core. The vortex center coincides with the center of the magnetic texture in (a) but is shifted away in (b).

the MZM from the superconducting Dirac fermion proposed by Fu-Kane applies [38]. This is further confirmed in Figs 2(c) and 2(d), where a finite $\mu > g_s$ crosses the continuous states, and the MZM always exists in the vortex core. However, for the $\mu > g_s$ case, the system is gapless for finite ℓ when $g_s > \Delta_0$ as shown in Fig. 2(d). We further calculate the vortex case $\Delta_0(r)e^{i\theta}$ and $g_s < 0$ [37], where the MZM exists $|g_s| < |\Delta_0|$ and disappears for $|g_s| > |\Delta_0|$. The subtle difference between positive and negative g_s in the vortex case can be seen from the analytic solution. In the limit of $\epsilon_0 \to 0$, the vortex core (where Δ_0 vanishes) can be taken to have a negligible size and the boundary condition at $r \to 0$ is unimportant, so the analytic zero-energy MZM solution is

$$\gamma_{0,+}^{\dagger} = (1, 0, 0, 1)^T \exp\left(-\int_0^r dr' \frac{\Delta_0(r') + g_s}{v_F}\right). \quad (14)$$

The solution is unphysical at $r \to \infty$ when $g_s < -\Delta_0 < 0$. For an antivortex $\Delta_0(r)e^{-i\theta}$, the MZM solution is $\gamma_{0,-}^{\dagger} = (0, 1, -1, 0)^T \exp(-\int_0^r dr'[\Delta_0(r') - g_s]/v_F)$. This represents that the MZM is from the consistent phase winding between $\Delta(\mathbf{r})$ and the magnetic texture $\boldsymbol{\mathcal{A}}_1$.

Now we understand that the radial magnetic texture effectively acts as an Abrikosov vortex, where the Abrikosov vortex core is at the center of the magnetic texture. We put the Dirac surface state on a sphere, and assume magnetic vortex ($g_s > 0$) and antivortex ($g_s < 0$) pairs are located at the north and south poles, respectively. In Fig. 3(a), when the flux line of the effective Abrikosov vortex penetrates the two poles, the pairing potential is $\Delta_0(r)e^{i\theta}$ and $\Delta_0(r)e^{-i\theta}$ locally at the north and south poles, respectively. The solutions for the MZM at the north and south poles are exactly the same, as they are time-reversal partners of each other. Now in the case of a weak exchange interaction g_s, where the radial magnetic texture could not contribute to a flux quantum, we need to add an external magnetic field to generate an Abrikosov vortex. If the external generated Abrikosov vortex core coincides with the center of the magnetic texture, the MZM locates at the north and south poles. Now the flux line is adiabatically shifted away from the south pole to point Z in Fig. 3(b). For the condition when the BdG spectrum has a full gap with a vortex-free pairing potential (which is $g_s < \Delta_0$, illustrated in SM [37]), then the MZMs, if they exist, can only be localized at the Abrikosov vortex core, since away from the vortex core the surface spectrum is gapped. Also, the condition for existence of MZMs in the vortex core at the Z point should be the same as that at the north pole ($g_s < \Delta_0$), otherwise it will be contradictory to the fact that MZMs always come in pairs. This argument can also be understood in the limit when the Z point is far away from the origin of the magnetic textures, so then the magnetization is approximately uniform and parallel to the surface. The parallel in-plane exchange term shifts the Dirac point away from the Γ point in the perpendicular direction, and introduces a pair-breaking effect between states at $\mathbf{k}$ and $-\mathbf{k}$. The superconducting surface states remain topological with a gap when $\Delta_0 > g_s$ [46], which is exactly the condition for the existence of MZMs in the vortex core. However, the adiabatical continuity fails when the BdG spectrum is gapless with a vortex-free pairing potential.

V. PHYSICAL REALIZATION

The above 2D magnetic texture has a singularity at the origin, while in ferromagnet films with a hard axis pointing along the z axis, a magnetic vortex with a spiraling magnetization configuration could emerge. $\mathbf{n}(\mathbf{r}) = (\cos\varphi\sqrt{1-n_z^2}, \sin\varphi\sqrt{1-n_z^2}, n_z)$, where $n_z(r)$ depends only on $r = \sqrt{x^2+y^2}$, $\varphi = q\phi + \phi_0$. The radial vortex $q = 1$, $\phi_0 = 0$ is a stabilized interfacial Dzyaloshinskii-Moriya interaction (DMI) [47], while a curling vortex $q = 0$, $\phi_0 = -\pi/2$ is obtained by minimizing the dipolar interactions [48,49]. They are the same as those in Figs. 1(a) and 1(b) at large r, respectively. Generally, $n_z(0) = 1$ and decays to $n(\xi_0) = 0$ within the decay length ξ_0, where a typical form is $n_z(r) = \mathrm{sech}(r/\xi_0)$ with $\xi_0 \approx 5$–10 nm. As long as $a > \xi_0$, the above study applies to the coupling between the Dirac electron and such a realistic magnetic vortex. Here, a is the size of the magnetic vortex within which a flux quantum is obtained. The bound state located at $r_{\max}$ may be probed by scanning tunneling microscopy. For an estimation, take $v_F \approx 5 \times 10^5$ m/s in Bi_2Te_3, then $a \approx 30$ nm when $g_s = 11$ meV.

We propose an artificial two-bilayer ferromagnet heterostructure to create a magnetic radial vortex, where the dipolar energy is minimized by an antiferromagnetic coupling between them and the radial vortex is obtained by the DMI gradient along the radial direction, namely the DMI parameter monotonically decreases as r increases. Another potential system is an intrinsic magnetic TI, where a magnetic texture is formed on the surface layer, for example, the spiral or skyrmion phases have been proposed as competing magnetic orders in $MnBi_2Te_4$ [50].

The incorporation of the magnetic proximity effect into a TI has been exemplified in heterostructures with magnetic insulators [51–53]. Recently, a van der Waals magnetic TI $MnBi_2Te_4$ and its descendants have been discovered [54–59], which is compatible with the Bi_2Te_3 family of materials. Furthermore, superconductors MoRe, $NbSe_2$, and Nb show a good proximity effect with TIs [60,61]. Such experimental progress on the material growth and rich material choice of TIs and magnetic insulators make it possible to realize a magnetic vortex in TI heterostructures.

ACKNOWLEDGMENTS

We acknowledge Jiang Xiao for valuable discussions. This work is supported by the National Key Research

Program of China under Grant No. 2019YFA0308404, the Natural Science Foundation of China through Grants No. 11774065 and No. 12174066, the Innovation Program for Quantum Science and Technology through Grant No. 2021ZD0302600, Science and Technology Commission of Shanghai Municipality under Grant No. 20JC1415900, and the Natural Science Foundation of Shanghai under Grant No. 19ZR1471400. C.W. is supported by the Natural Science Foundation of China through Grants No. 12174317 and No. 11729402.

[1] M. Z. Hasan and C. L. Kane, *Colloquium*: Topological insulators, Rev. Mod. Phys. **82**, 3045 (2010).
[2] X.-L. Qi and S.-C. Zhang, Topological insulators and superconductors, Rev. Mod. Phys. **83**, 1057 (2011).
[3] Y. Tokura, K. Yasuda, and A. Tsukazaki, Magnetic topological insulators, Nat. Rev. Phys. **1**, 126 (2019).
[4] J. Wang and S.-C. Zhang, Topological states of condensed matter, Nat. Mater. **16**, 1062 (2017).
[5] W. Yang, C. Xu, and C. Wu, Single branch of chiral Majorana modes from doubly degenerate Fermi surfaces, Phys. Rev. Research **2**, 042047(R) (2020).
[6] X.-L. Qi, T. L. Hughes, and S.-C. Zhang, Topological field theory of time-reversal invariant insulators, Phys. Rev. B **78**, 195424 (2008).
[7] R. Yu, W. Zhang, H.-J. Zhang, S.-C. Zhang, X. Dai, and Z. Fang, Quantized anomalous Hall effect in magnetic topological insulators, Science **329**, 61 (2010).
[8] C.-Z. Chang, J. Zhang, X. Feng, J. Shen, Z. Zhang, M. Guo, K. Li, Y. Ou, P. Wei, L.-L. Wang, Z.-Q. Ji, Y. Feng, S. Ji, X. Chen, J. Jia, X. Dai, Z. Fang, S.-C. Zhang, K. He, Y. Wang *et al.*, Experimental observation of the quantum anomalous Hall effect in a magnetic topological insulator, Science **340**, 167 (2013).
[9] J. G. Checkelsky, R. Yoshimi, A. Tsukazaki, K. S. Takahashi, Y. Kozuka, J. Falson, M. Kawasaki, and Y. Tokura, Trajectory of the anomalous Hall effect towards the quantized state in a ferromagnetic topological insulator, Nat. Phys. **10**, 731 (2014).
[10] X. Kou, S.-T. Guo, Y. Fan, L. Pan, M. Lang, Y. Jiang, Q. Shao, T. Nie, K. Murata, J. Tang, Y. Wang, L. He, T.-K. Lee, W.-L. Lee, and K. L. Wang, Scale-Invariant Quantum Anomalous Hall Effect in Magnetic Topological Insulators beyond the Two-Dimensional Limit, Phys. Rev. Lett. **113**, 137201 (2014).
[11] A. J. Bestwick, E. J. Fox, X. Kou, L. Pan, K. L. Wang, and D. Goldhaber-Gordon, Precise Quantization of the Anomalous Hall Effect near Zero Magnetic Field, Phys. Rev. Lett. **114**, 187201 (2015).
[12] Y. Deng, Y. Yu, M. Z. Shi, Z. Guo, Z. Xu, J. Wang, X. H. Chen, and Y. Zhang, Quantum anomalous Hall effect in intrinsic magnetic topological insulator $MnBi_2Te_4$, Science **367**, 895 (2020).
[13] J. Wang, B. Lian, and S.-C. Zhang, Quantum anomalous Hall effect in magnetic topological insulators, Phys. Scr. **T164**, 014003 (2015).
[14] C.-X. Liu, S.-C. Zhang, and X.-L. Qi, The quantum anomalous Hall effect: Theory and experiment, Annu. Rev. Condens. Matter Phys. **7**, 301 (2016).
[15] J. Wang, B. Lian, X.-L. Qi, and S.-C. Zhang, Quantized topological magnetoelectric effect of the zero-plateau quantum anomalous Hall state, Phys. Rev. B **92**, 081107(R) (2015).
[16] M. Mogi, M. Kawamura, R. Yoshimi, A. Tsukazaki, Y. Kozuka, N. Shirakawa, K. S. Takahashi, M. Kawasaki, and Y. Tokura, A magnetic heterostructure of topological insulators as a candidate for an axion insulator, Nat. Mater. **16**, 516 (2017).
[17] M. Mogi, M. Kawamura, A. Tsukazaki, R. Yoshimi, K. S. Takahashi, M. Kawasaki, and Y. Tokura, Tailoring tricolor structure of magnetic topological insulator for robust axion insulator, Sci. Adv. **3**, eaao1669 (2017).
[18] S. Grauer, K. M. Fijalkowski, S. Schreyeck, M. Winnerlein, K. Brunner, R. Thomale, C. Gould, and L. W. Molenkamp, Scaling of the Quantum Anomalous Hall Effect as an Indicator of Axion Electrodynamics, Phys. Rev. Lett. **118**, 246801 (2017).
[19] D. Xiao, J. Jiang, J.-H. Shin, W. Wang, F. Wang, Y.-F. Zhao, C. Liu, W. Wu, M. H. W. Chan, N. Samarth, and C.-Z. Chang, Realization of the Axion Insulator State in Quantum Anomalous Hall Sandwich Heterostructures, Phys. Rev. Lett. **120**, 056801 (2018).
[20] C. Liu, Y. Wang, H. Li, Y. Wu, Y. Li, J. Li, K. He, Y. Xu, J. Zhang, and Y. Wang, Robust axion insulator and Chern insulator phases in a two-dimensional antiferromagnetic topological insulator, Nat. Mater. **19**, 522 (2020).
[21] K. N. Okada, Y. Takahashi, M. Mogi, R. Yoshimi, A. Tsukazaki, K. S. Takahashi, N. Ogawa, M. Kawasaki, and Y. Tokura, Terahertz spectroscopy on Faraday and Kerr rotations in a quantum anomalous Hall state, Nat. Commun. **7**, 12245 (2016).
[22] L. Wu, M. Salehi, N. Koirala, J. Moon, S. Oh, and N. P. Armitage, Quantized Faraday and Kerr rotation and axion electrodynamics of a 3D topological insulator, Science **354**, 1124 (2016).
[23] V. Dziom, A. Shuvaev, A. Pimenov, G. V. Astakhov, C. Ames, K. Bendias, J. Böttcher, G. Tkachov, E. M. Hankiewicz, C. Brüne, H. Buhmann, and L. W. Molenkamp, Observation of the universal magnetoelectric effect in a 3D topological insulator, Nat. Commun. **8**, 15197 (2017).
[24] I. Garate and M. Franz, Inverse Spin-Galvanic Effect in the Interface between a Topological Insulator and a Ferromagnet, Phys. Rev. Lett. **104**, 146802 (2010).
[25] K. Nomura and N. Nagaosa, Electric charging of magnetic textures on the surface of a topological insulator, Phys. Rev. B **82**, 161401(R) (2010).
[26] T. Yokoyama, J. Zang, and N. Nagaosa, Theoretical study of the dynamics of magnetization on the topological surface, Phys. Rev. B **81**, 241410(R) (2010).
[27] Y. Tserkovnyak and D. Loss, Thin-Film Magnetization Dynamics on the Surface of a Topological Insulator, Phys. Rev. Lett. **108**, 187201 (2012).
[28] H. M. Hurst, D. K. Efimkin, J. Zang, and V. Galitski, Charged skyrmions on the surface of a topological insulator, Phys. Rev. B **91**, 060401(R) (2015).
[29] D. Andrikopoulos, B. Sorée, and J. De Boeck, Skyrmion-induced bound states on the surface of three-dimensional topological insulators, J. Appl. Phys. **119**, 193903 (2016).
[30] D. J. Thouless, *Topological Quantum Numbers in Nonrealistic Physics* (World Scientific, Singapore, 1998).
[31] X. L. Yang, S. H. Guo, F. T. Chan, K. W. Wong, and W. Y. Ching, Analytic solution of a two-dimensional hydrogen atom. I. Nonrelativistic theory, Phys. Rev. A **43**, 1186 (1991).
[32] D. G. W. Parfitt and M. E. Portnoi, The two-dimensional hydrogen atom revisited, J. Math. Phys. **43**, 4681 (2002).

[33] Y. Li, X. Zhou, and C. Wu, Two- and three-dimensional topological insulators with isotropic and parity-breaking Landau levels, Phys. Rev. B **85**, 125122 (2012).

[34] X. Zhou, Y. Li, Z. Cai, and C. Wu, Unconventional states of bosons with the synthetic spin–orbit coupling, J. Phys. B: At., Mol. Opt. Phys. **46**, 134001 (2013).

[35] Y. Aharonov and A. Casher, Ground state of a spin-1/2 charged particle in a two-dimensional magnetic field, Phys. Rev. A **19**, 2461 (1979).

[36] N. Hayashi, T. Isoshima, M. Ichioka, and K. Machida, Low-Lying Quasiparticle Excitations around a Vortex Core in Quantum Limit, Phys. Rev. Lett. **80**, 2921 (1998).

[37] See Supplemental Material at http://link.aps.org/supplemental/10.1103/PhysRevB.106.035134 for technical details.

[38] L. Fu and C. L. Kane, Superconducting Proximity Effect and Majorana Fermions at the Surface of a Topological Insulator, Phys. Rev. Lett. **100**, 096407 (2008).

[39] P. Hosur, P. Ghaemi, R. S. K. Mong, and A. Vishwanath, Majorana Modes at the Ends of Superconductor Vortices in Doped Topological Insulators, Phys. Rev. Lett. **107**, 097001 (2011).

[40] J.-P. Xu, M.-X. Wang, Z. L. Liu, J.-F. Ge, X. Yang, C. Liu, Z. A. Xu, D. Guan, C. L. Gao, D. Qian, Y. Liu, Q.-H. Wang, F.-C. Zhang, Q.-K. Xue, and J.-F. Jia, Experimental Detection of a Majorana Mode in the Core of a Magnetic Vortex Inside a Topological Insulator-Superconductor $Bi_2Te_3/NbSe_2$ Heterostructure, Phys. Rev. Lett. **114**, 017001 (2015).

[41] G. Xu, B. Lian, P. Tang, X.-L. Qi, and S.-C. Zhang, Topological Superconductivity on the Surface of Fe-Based Superconductors, Phys. Rev. Lett. **117**, 047001 (2016).

[42] D. Wang, L. Kong, P. Fan, H. Chen, S. Zhu, W. Liu, L. Cao, Y. Sun, S. Du, J. Schneeloch, R. Zhong, G. Gu, L. Fu, H. Ding, and H.-J. Gao, Evidence for Majorana bound states in an iron-based superconductor, Science **362**, 333 (2018).

[43] K. Jiang, X. Dai, and Z. Wang, Quantum Anomalous Vortex and Majorana Zero Mode in Iron-Based Superconductor Fe(Te,Se), Phys. Rev. X **9**, 011033 (2019).

[44] S. S. Pershoguba, S. Nakosai, and A. V. Balatsky, Skyrmion-induced bound states in a superconductor, Phys. Rev. B **94**, 064513 (2016).

[45] G. Yang, P. Stano, J. Klinovaja, and D. Loss, Majorana bound states in magnetic skyrmions, Phys. Rev. B **93**, 224505 (2016).

[46] N. F. Q. Yuan and L. Fu, Zeeman-induced gapless superconductivity with a partial Fermi surface, Phys. Rev. B **97**, 115139 (2018).

[47] G. Siracusano, R. Tomasello, A. Giordano, V. Puliafito, B. Azzerboni, O. Ozatay, M. Carpentieri, and G. Finocchio, Magnetic Radial Vortex Stabilization and Efficient Manipulation Driven by the Dzyaloshinskii-Moriya Interaction and Spin-Transfer Torque, Phys. Rev. Lett. **117**, 087204 (2016).

[48] T. Shinjo, T. Okuno, R. Hassdorf, K. Shigeto, and T. Ono, Magnetic vortex core observation in circular dots of permalloy, Science **289**, 930 (2000).

[49] A. Wachowiak, J. Wiebe, M. Bode, O. Pietzsch, M. Morgenstern, and R. Wiesendanger, Direct observation of internal spin structure of magnetic vortex cores, Science **298**, 577 (2002).

[50] B. Li, J.-Q. Yan, D. M. Pajerowski, E. Gordon, A.-M. Nedić, Y. Sizyuk, L. Ke, P. P. Orth, D. Vaknin, and R. J. McQueeney, Competing Magnetic Interactions in the Antiferromagnetic Topological Insulator $MnBi_2Te_4$, Phys. Rev. Lett. **124**, 167204 (2020).

[51] P. Wei, F. Katmis, B. A. Assaf, H. Steinberg, P. Jarillo-Herrero, D. Heiman, and J. S. Moodera, Exchange-Coupling-Induced Symmetry Breaking in Topological Insulators, Phys. Rev. Lett. **110**, 186807 (2013).

[52] F. Katmis, V. Lauter, F. S. Nogueira, B. A. Assaf, M. E. Jamer, P. Wei, B. Satpati, J. W. Freeland, I. Eremin, D. Heiman, P. Jarillo-Herrero, and J. S. Moodera, A high-temperature ferromagnetic topological insulating phase by proximity coupling, Nature (London) **533**, 513 (2016).

[53] C. Tang, C.-Z. Chang, G. Zhao, Y. Liu, Z. Jiang, C.-X. Liu, M. R. McCartney, D. J. Smith, T. Chen, J. S. Moodera, and J. Shi, Above 400-K robust perpendicular ferromagnetic phase in a topological insulator, Sci. Adv. **3**, e1700307 (2017).

[54] D. Zhang, M. Shi, T. Zhu, D. Xing, H. Zhang, and J. Wang, Topological Axion States in the Magnetic Insulator $MnBi_2Te_4$ with the Quantized Magnetoelectric Effect, Phys. Rev. Lett. **122**, 206401 (2019).

[55] M. M. Otrokov, I. I. Klimovskikh, H. Bentmann, D. Estyunin, A. Zeugner, Z. S. Aliev, S. Gaß, A. U. B. Wolter, A. V. Koroleva, A. M. Shikin, M. Blanco-Rey, M. Hoffmann, I. P. Rusinov, A. Yu. Vyazovskaya, S. V. Eremeev, Yu. M. Koroteev, V. M. Kuznetsov, F. Freyse, J. Sánchez-Barriga, I. R. Amiraslanov *et al.*, Prediction and observation of an antiferromagnetic topological insulator, Nature (London) **576**, 416 (2019).

[56] Y. Gong, J. Guo, J. Li, K. Zhu, M. Liao, X. Liu, Q. Zhang, L. Gu, L. Tang, X. Feng, D. Zhang, W. Li, C. Song, L. Wang, P. Yu, X. Chen, Y. Wang, H. Yao, W. Duan, Y. Xu *et al.*, Experimental realization of an intrinsic magnetic topological insulator, Chin. Phys. Lett. **36**, 076801 (2019).

[57] J. Wu, F. Liu, M. Sasase, K. Ienaga, Y. Obata, R. Yukawa, K. Horiba, H. Kumigashira, S. Okuma, T. Inoshita, and H. Hosono, Natural van der Waals heterostructural single crystals with both magnetic and topological properties, Sci. Adv. **5**, eaax9989 (2019).

[58] J.-Q. Yan, Y. H. Liu, D. S. Parker, Y. Wu, A. A. Aczel, M. Matsuda, M. A. McGuire, and B. C. Sales, A-type antiferromagnetic order in $MnBi_4Te_7$ and $MnBi_6Te_{10}$ single crystals, Phys. Rev. Materials **4**, 054202 (2020).

[59] C. Hu, L. Ding, K. N. Gordon, B. Ghosh, H.-J. Tien, H. Li, A. G. Linn, S.-W. Lien, C.-Y. Huang, S. Mackey, J. Liu, P. V. S. Reddy, B. Singh, A. Agarwal, A. Bansil, M. Song, D. Li, S.-Y. Xu, H. Lin, H. Cao *et al.*, Realization of an intrinsic ferromagnetic topological state in $MnBi_8Te_{13}$, Sci. Adv. **6**, eaba4275 (2020).

[60] M.-X. Wang, C. Liu, J.-P. Xu, F. Yang, L. Miao, M.-Y. Yao, C. L. Gao, C. Shen, X. Ma, X. Chen, Z.-A. Xu, Y. Liu, S.-C. Zhang, D. Qian, J.-F. Jia, and Q.-K. Xue, The coexistence of superconductivity and topological order in the Bi_2Se_3 thin films, Science **336**, 52 (2012).

[61] W.-X. Wu, Y. Feng, Y.-H. Bai, Y.-Y. Jiang, Z.-W. Gao, Y.-Z. Li, J.-L. Luan, H.-A. Zhou, W.-J. Jiang, X. Feng, J.-S. Zhang, H. Zhang, K. He, X.-C. Ma, Q.-K. Xue, and Y.-Y. Wang, Gate tunable supercurrent in Josephson junctions based on Bi_2Te_3 topological insulator thin films, Chin. Phys. Lett. **38**, 037402 (2021).